HHS Public Access

Author manuscript

ACS Chem Biol. Author manuscript; available in PMC 2019 February 11.

Published in final edited form as:

ACS Chem Biol. 2018 July 20; 13(7): 1844–1852. doi:10.1021/acschembio.7b00748.

Tuning the Color Palette of Fluorescent Copper Sensors through Systematic Heteroatom Substitution at Rhodol Cores

Shang Jia[†,⊥], **Karla M. Ramos-Torres**[†,⊥], **Safacan Kolemen**[†,‡], **Cheri M. Ackerman**[†], and **Christopher J. Chang**[*,†,§,‖]

[†]Department of Chemistry, University of California, Berkeley, California 94720, United States

[‡]Department of Chemistry, Koc University, Rumelifeneri Yolu, 34450, Sariyer, Istanbul, Turkey

[§]Department of Molecular and Cell Biology, University of California, Berkeley, California 94720, United States

[‖]Howard Hughes Medical Institute, University of California, Berkeley, California 94720, United States

Abstract

Copper is an essential nutrient for sustaining life, and emerging data have expanded the roles of this metal in biology from its canonical functions as a static enzyme cofactor to dynamic functions as a transition metal signal. At the same time, loosely bound, labile copper pools can trigger oxidative stress and damaging events that are detrimental if misregulated. The signal/stress dichotomy of copper motivates the development of new chemical tools to study its spatial and temporal distributions in native biological contexts such as living cells. Here, we report a family of fluorescent copper sensors built upon carbon-, silicon-, and phosphorus-substituted rhodol dyes that enable systematic tuning of excitation/emission colors from orange to near-infrared. These probes can detect changes in labile copper levels in living cells upon copper supplementation and/or depletion. We demonstrate the ability of the carbon-rhodol based congener, Copper Carbo Fluor 1 (CCF1), to identify elevations in labile copper pools in the Atp7a$^{-/-}$ fibroblast cell model of the genetic copper disorder Menkes disease. Moreover, we showcase the utility of the red-emitting phosphorus-rhodol based dye Copper Phosphorus Fluor 1 (CPF1) in dual-color, dual-analyte imaging experiments with the green-emitting calcium indicator Calcium Green-1 to enable simultaneous detection of fluctuations in copper and calcium pools in living cells. The results provide a starting point for advancing tools to study the contributions of copper to health and disease and for exploiting the rapidly growing palette of heteroatom-substituted xanthene dyes to rationally tune the optical properties of fluorescent indicators for other biologically important analytes.

[*]**Corresponding Author** Phone: 001-(510)642-4704. chrischang@berkeley.edu. Twitter: @christhechang.

[⊥]Author Contributions

These authors contributed equally to this work and are listed in alphabetical order by last name.

Supporting Information

The Supporting Information is available free of charge on the ACS Publications website at DOI: 10.1021/acschembio.7b00748. Supplementary characterization and imaging results of CXF probes, experimental methods, and synthesis and characterization of all compounds (PDF)

The authors declare no competing financial interest.

Graphical Abstract

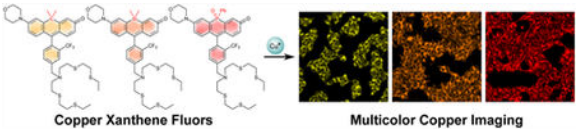

Copper is an indispensable element for life.[1,2] The redox capacity of this transition metal is widely exploited as a catalytic and structural cofactor in proteins that spans a diverse array of fundamental processes including oxygen transport, respiration and metabolism, cell growth and differentiation, and signal transduction.[1–5] Conversely, copper dysregulation can lead to cellular malfunctions resulting from the aberrant production of reactive oxygen species (ROS) and subsequent oxidative damage to proteins, lipids, and DNA/RNA.[6,7] Indeed, organisms have evolved cellular machineries to carefully regulate copper uptake, transport, storage, and excretion,[8–13] and irregular deviations from this delicate balance have been linked to pathogenic states including neurodegenerative disorders like Alzheimer's,[14–17] Parkinson's,[18] and Huntington's[19] diseases and familial amyotrophic lateral sclerosis,[20–23] metabolic disorders such as diabetes and obesity,[24–26] and genetic disorders like Menkes[27,28] and Wilson's[29–31] diseases. In addition, emerging data from our laboratory and others have revealed that dynamic copper fluxes can also regulate essential physiological functions[32,33] spanning metabolic processes such as lipolysis;[5] neural processes such as spontaneous activity,[34] neuronal calcium signaling,[35] and olfaction;[36,37] as well as kinase pathways involved in signaling and tumorogenesis.[3,4]

The broad contributions of copper to health and disease motivate the development of technologies to help disentangle its disparate physiological and pathological effects. In this context, the use of fluorescent sensors for visualizing metal fluxes has proven to be a potentially powerful strategy for studying these elements in their native biological contexts with spatial and temporal resolution.[32,33,38–44] This approach is well- suited for the simultaneous study of multiple biological events using different probes as long as spectral overlap between chromophores is sufficiently minimized.[39,45–48] With specific regard to copper, a growing toolbox of small-molecule[44,49–51] and macromolecular[52–55] fluorescent probes for this essential metal have emerged for use in cells and more complex biological specimens. Moreover, application of these chemical reagents in conjunction with other direct imaging techniques as well as supporting biochemical and cell biology studies have identified new copper biology in bacterial,[56,57] yeast,[58–60] plant,[61] worm,[62] and mammalian[63–66] models. Included are examples of activity-dependent neuronal copper translocation,[34] copper-dependent antimicrobial behavior,[57,67,68] hyper-accumulation of copper in cuprosome organelles triggered by zinc deficiency,[69] and copper-regulated lipolysis.[5] Despite this progress, the base fluorophores for fluorescent copper detection have relied on a variety of scaffolds, ranging from UV-excitable pyrazoline[70–72] and naphthalene,[73] visible-wavelength BODIPY[35,74,75] and rhodol,[34] to far-red silicon rhodol[5] and near-infrared cyanine dyes,[76,77] which presents a unique challenge for optimizing the combination of copper-selective recognition elements exhibiting high metal and redox specificity along with dye platforms allowing for fine control of excitation/emission color profiles.

Against this backdrop, we sought to pursue an alternative strategy in which rational tuning of probe excitation/emission colors of fluorescent copper sensors could be achieved independently of the metal-responsive moiety. In particular, we were inspired by elegant studies that have greatly expanded the optical spectral window of xanthene-based fluorophores like fluorescein, rhodamine, and rhodol[78–90] and thus turned our attention to reports on substitution of the endocyclic oxygen atom in the xanthene core of green-fluorescent fluorescein by carbon, silicon, or phosphorus to provide new red-shifted fluorophores with emission profiles from the orange to near-infrared region,[82,86,88] yielding improved tissue penetration and minimized sample photodamage.[91] We now report the development of the Copper Xanthene Fluor (CXF) family of copper-responsive fluorescent indicators based on carbon (Copper Carbo Fluor 1, CCF1), silicon (Copper Silicon Fluor 1, CSF1), and phosphorus (Copper Phosphorus Fluor 1, CPF1) analogs of the rhodol-based Copper Fluor series,[34] along with matched control dyes that possess the same fluorophore scaffolds but feature isosteric sulfur-to-carbon substitutions along the receptor portion to render them nonresponsive to copper. We establish the utility of these CXF dyes to visualize changes in labile copper pools in HEK 293T cells with copper supplementation and/or chelation. Moreover, the CCF1 probe is capable of distinguishing elevations in labile copper levels in the Menkes Atp7a$^{-/-}$ fibroblast cell model from normal levels in wildtype controls. Finally, the most red-shifted probe of the series, CPF1, enables dual-color, dual-analyte imaging of copper and calcium pools in conjunction with the green-emitting dye Calcium Green-1.

RESULTS AND DISCUSSION

Design and Synthesis of a Color Palette of Fluorescent Copper Probes Based on Center-Atom Substitution of the Rhodol Core.

Inspired by emerging progress on the development of new fluorophores derived from center-atom substitution of the xanthene oxygen of classic fluorescein and rhodamine dyes, we envisioned generating a series of red-shifted fluorescent copper sensors by transforming rhodol scaffolds employed in our recently reported Copper Rhodol (CR) and Copper Fluor (CF) family into carbon, silicon, and phosphorus-substituted analogs.[5,34] The synthesis and structures of the fluorescent copper indicators, CCF1, CSF1, and CPF1, along with control dyes that are not responsive to copper, are depicted in Scheme 1. In particular, our design makes use of a trifluoromethyl (CF_3) group on the pendant aryl ring attached to the xanthene backbone, as previous work from our laboratory establishes that substitution of a methyl for trifluoromethyl at this position leads to enhancements in both the dynamic range and optical brightness of rhodol-based copper probes by decreasing the available nonradiative decay pathways from rotational motions about the aryl–aryl bond.[34] We also synthesized matched control dyes, Ctrl-CCF1, Ctrl-CSF1, and Ctrl-CPF1, which are non-responsive to Cu^+ due to the replacement of the thioether motifs by methylene units in the metal-binding domain (Scheme 1). These control dyes can be used in parallel imaging experiments to distinguish copper-dependent responses from potential dye-dependent variations, which could include cellular uptake, trappability, and subcellular accumulation as well as changes in pH, redox, and hydrophobic/hydrophilic environments.

Spectroscopic Properties of CXF Copper Sensors.

We first sought to evaluate the optical responses of the CXF series and their control analogs to copper in spectrophotometric assays. As anticipated, all three copper probes showed turn-on responses upon treatment with Cu^+ in an aqueous solution buffered to physiological pH, with a ca. 17-fold increase for CSF1, 5-fold increase for CCF1, and 7-fold increase for CPF1 (Figure 1a,c,e). We speculate that the observed differences in turn-on ratios between the three probes may result from various factors, including photoinduced electron transfer (PeT) quenching efficiency, variations in rotational freedom on the receptor upon Cu^+ binding, as well as changes in other nonradiative relaxation pathways that become more prominent with a smaller HOMO–LUMO gap as supported by the lower quantum yields of CSF1 and CPF1 (Table 1).

The copper-binding affinities of these probes are within the expected range for small-molecule fluorescent copper indicators with thioether-rich ligand sets,[50,51] with CPF1 having the strongest affinity and CSF1 being the weakest Cu^+ binder (Figures S1b,c, S2b,c, and S3b,c). The apparent K_d values for CCF1, CSF1, and CPF1 are 0.20, 0.49, and 0.02 pM, respectively, and all show a 1:1 Cu/dye binding ratio. Additionally, all three probes show excellent selectivity for Cu^+ over various biologically relevant metal ions (Figure 1b,d,f) and maintain their effective turn-on responses to Cu^+ over a physiological pH range (Figure S1d, S2d and S3d). We observe a slight turn-on effect from Cu^{2+}, which most likely results from the slow reduction of Cu^{2+} to Cu^+ upon interaction with the sulfur-rich receptor (Figure S3i). In contrast, the control dyes, Ctrl-CCF1, Ctrl-CSF1, and Ctrl-CPF1, do not exhibit any metal-dependent responses.

The spectral properties of the three probe-control pairs are listed in Table 1. As expected, all three sets show lower energy excitation and emission wavelengths compared to the rhodol-based congeners Copper Fluor 3 (CF3) and Control Copper Fluor 3 (Ctrl-CF3),[34] with the CCF1/Ctrl-CCF1 pair showing the smallest bathochromic shift (20–40 nm) and the CPF1/Ctrl-CPF1 pair exhibiting the most red-shifted spectra (80–100 nm) relative to the oxygen-based rhodol, which is in line with what is observed for carbon-, silicon-, and phosphorus-based derivatives of fluorescein.[90] Because of the nature of the rhodol scaffold as a fluorescein-rhodamine hybrid, these probes exhibit a relatively broad absorption profile (full width at half-maximum [fwhm] greater than 145 nm for apo-CXF and above 90 nm for copper-bound CXF indicators, Figures S1a, S2a, and S3a), which can pose potential limitations for some multicolor, multianalyte imaging experiments. However, the relatively narrow profiles of the emission peaks for these dyes (fwhm = 44 nm for CCF1 and CPF1, 34 nm for CSF1) balance their absorption behavior and provide an opportunity to use probes with a longer emission wavelength, such as the phosphorus rhodol-based sensor CPF1, in dual-channel imaging experiments through disentangling distinct emission signals.

Finally, to further characterize the spectroscopic properties of this new CXF series of dyes, we assessed their ability to respond to copper in aqueous buffer with additives to mimic aspects of more complex biological environments. Specifically, we evaluated the response of the probes in buffer with BSA as a model protein or 1,2-dimyrisotyl-sn-glycero-3-phosphocholine (DMPC) as a model lipid, as well as whole cell lysates. As expected, both the CXF probes and their Ctrl-CXF analogs do show some background fluorescence with

these in vitro additives. However, only the CXF indicators, but not the Ctrl-CXF dyes, respond to Cu^{+} addition through a turn-on response over the background, and more importantly, the observed copper-dependent fluorescence increases can be reversibly turned off by the addition of competing copper chelators. Indeed, Ctrl-CXF control dyes display a minimal response to such copper supplementation and/or depletion treatments (Figure S1e–h, S2e–h, and S3e–h). Taken together, the data establish that the CCF1, CSF1, and CPF1 indicators, when used in conjunction with their Ctrl-CXF control analogs, are effective chemical tools for turn-on fluorescence detection of copper in an aqueous buffer as well as in whole cell lysates.

Live-Cell Imaging of Changes in Labile Copper Pools in HEK 293T Models.

With these spectroscopic data in hand, we next evaluated the ability of the CXF probes to visualize changes in labile copper pools in cell culture models. To this end, we treated human embryonic kidney (HEK 293T) cells for 12 h with either 100 μM $CuCl_2$ to increase intracellular copper concentrations or 500 μM bathocuproine sulfonate (BCS), a membrane-impermeable copper chelator, to deplete endogenous labile copper pools and then labeled with CXF or Ctrl-CXF probes for live-cell imaging experiments (Figure 2). As anticipated, HEK 293T cells stained with CCF1, CSF1, and CPF1 all showed increased intracellular fluorescence under copper supplementation conditions relative to vehicle control cells, with CPF1 having the highest turn-on signal-to-noise ratio of the three copper indicators, in line with its highest Cu^{+} binding affinity observed in spectroscopic assays. We observed that only CCF1 and CPF1, but not CSF1, showed a slight but statistically significant fluorescence decrease in HEK 293T cells treated with the BCS chelator that induces labile copper deficiency relative to the vehicle control. The cellular distribution patterns of CXF reagents were similar for all conditions tested, and further co-staining experiments with fluorescent markers for organelles suggest overlap with the endoplasmic reticulum (ER; Figure S4). In further agreement with in vitro spectroscopic studies, all of the Ctrl-CXF control dyes did not show significant differences in fluorescence intensity with either copper supplementation or depletion, further validating that the CXF indicators can be used to report changes in labile copper status in living cells. The results from these initial cell studies suggest that the CSF1/Ctrl-CSF1 pair in particular might be more effective in applications for the detection of increases in labile cellular copper levels, whereas the CCF1/Ctrl-CCF1 and CPF1/Ctrl-CPF1 pairs may be used to visualize either depletions or accumulations of labile cellular copper pools relative to basal levels.

Application of CCF1/Ctrl-CCF1 to Detect Elevations in Labile Copper Pools in the Atp7a Knockout Fibroblast Cell Model of Menkes Disease.

We next sought to apply the CXF reagents to identify and assess aberrant changes in labile copper pools in cell-based models of disease. To this end, we utilized $Atp7a^{-/-}$ mouse embryonic fibroblasts (MEFs), a model that mimics genetic copper misregulation in Menkes disease.[28,62,93] Atp7a is a major copper transporter protein that regulates secretion and export of excess copper to maintain copper homeostasis,[12] and deletion and/or loss-of-function mutations results in hyperaccumulation of copper compared to the wild type.[94,95] Indeed, we confirmed by ICP-MS measurements that MEF $Atp7a^{-/-}$ cells possess over 6

times as much total copper as their genetically matched MEF wild-type cells in the cytoplasmic extract, and 2.6 times as much in the nucleus (Figure S5).

Owing to its superior dynamic range in response to copper supplementation experiments within cells, we utilized CCF1 to visualize labile copper pools in Atp7a$^{-/-}$ MEFs versus wild type (WT) congeners. As shown in Figure 3, CCF1-stained cells displayed statistically significant elevations in intracellular fluorescence in MEF Atp7a$^{-/-}$ cells compared to WT controls. Besides the observed increases in CCF1 fluorescence in Atp7a$^{-/-}$ compared to WT cells, Ctrl-CCF1 fluorescence intensities in Atp7a$^{-/-}$ cells are slightly lower than those in WT fibroblasts, suggesting lower dye uptake in Atp7a$^{-/-}$ cells. The collective imaging data identify that in addition to total copper levels, labile copper levels in the Atp7a KO cells are also higher than their WT counterparts.

Dual-Color Imaging with CPF1 and Calcium Green-1 Allows Simultaneous Detection of Labile Cellular Copper and Calcium Pools.

As an additional set of experiments to showcase the utility of an expanded color palette for the CXF family of copper sensors, we utilized the most red-shifted analog, CPF1, in dual-analyte, dual-color imaging experiments. CPF1 displays a deep red emission peak centered around 678 nm in the apo form and is essentially nonemissive below 600 nm, which makes it spectrally well-separated from common green-emitting fluorescent reporters like fluorescein and GFP. This feature of CPF1 enables simultaneous multicolor imaging of copper and other biologically relevant analytes and related targets.

To meet this goal, we performed dual-channel imaging of CPF1 alongside Calcium Green 1-AM, a fluorescein-based cell-trappable calcium indicator with green fluorescence. As expected, the green Calcium Green-1 and red CPF1 channels are spectrally well-separated (Figure 4). Live HEK 293T cells treated with 50 μM $CuCl_2$ overnight exhibited a selective increase of intracellular fluorescence in the copper-sensitive CPF1 red channel but not in the Calcium Green-1 green channel (Figure 4a–e). In contrast, treatment of HEK 293T cells with 1 μM of the calcium ionophore A23187, which can permeabilize the cell membrane and lead to calcium influx, resulted in enhanced fluorescence selectively in the Calcium Green-1 channel with no effect on fluorescence intensity in the CPF1 channel (Figure 4f–j). Similar results were obtained with dual-color imaging of Ctrl-CPF1 and Calcium Green-1, where the Ctrl-CPF1 red channel was nonresponsive to either copper supplementation or triggered calcium uptake and the Calcium Green-1 channel only responded to A23187-stimulated calcium influx (Figure S6). The results establish the red-shifted CPF1 and Ctrl-CPF1 as a valuable set of reagents to monitor changes in labile copper pools in combination with other fluorescent reporters for multichannel, multianalyte imaging experiments.

CONCLUSIONS

To close, we have presented the design, synthesis, and in vitro and *in cellulo* characterization of a homologous family of fluorescent copper probes along with matched control dye compounds that feature center-atom substitution of the rhodol fluorophore. Systematic modifications to the xanthene oxygen to generate carbon, silicon, and phosphorus rhodol analogs furnished a palette of copper sensors with a range of emission profiles that span the

orange to deep red region, while maintaining a general copper-binding receptor to confer high metal and redox specificity. The resulting probes are capable of detecting changes in labile copper pools in living cells, as illustrated by pilot studies in HEK 293T cells with copper supplementation and/or depletion. Importantly, the imaging studies are supported by comparison with matched control Ctrl-CXF analogs that are nonresponsive to copper fluctuations and can thus serve as reference compounds for potential dye-dependent responses. Moreover, imaging experiments with the carbon rhodol CCF1 and its Ctrl-CCF1 analog are consistent with elevations in labile copper pools in Atp7a$^{-/-}$ MEF cells lacking this central copper export protein compared to wild-type fibroblasts. Finally, the near-IR optical profile of the phosphorus-based CPF1 congener enables simultaneous, dual-color imaging of copper and calcium fluxes in living cells with high metal specificity. Collectively, this work shows that center-atom substitution of xanthene dyes can provide a general, rational strategy for expanding the color palette of fluorescent indicators while maintaining the same recognition/reactivity motif for analyte detection, along with providing reagents for advanced studies of copper biology.

METHODS

A description of general methods and materials for image analysis, cell fractionation, and inductively coupled plasma (ICP)-MS analysis, as well as full details on the synthesis and characterization of all compounds, is given in the SI.

Preparation of Cell Cultures.

Cells were grown in the Cell Culture Facility at the University of California, Berkeley. HEK 293T cells and MEF cells were cultured in DMEM supplemented with 10% FBS and glutamine (2 mM). Two days before imaging, cells were passed and plated on four-well chamber slides (Lab-Tek, Thermo Fisher Scientific) coated with poly-L-lysine (50 mg mL^{-1}, Sigma-Aldrich).

Cell Staining and Imaging.

Confocal fluorescence images were acquired with a Zeiss LSM710 laser-scanning microscope with a 20× objective lens. Excitation at 543 nm for CCF1/Ctrl-CCF1, 594 nm for CSF1/Ctrl-CSF1, 633 nm for CPF1/Ctrl-CPF1, and 488 nm for Calcium Green-1 was carried out with appropriate lasers. Cells were incubated with 2 μM CCF1/Ctrl-CCF1, CSF1/Ctrl-CSF1, and CPF1/Ctrl-CPF1 in DMEM without phenol red (Invitrogen) for 15 min at 37 °C under 5% CO_2, washed, and imaged in fresh DMEM without phenol red. For imaging of HEK 293T cells with copper addition or depletion, cells were treated with 50 μM $CuCl_2$, 500 μM BCS, or water in DMEM without phenol red for 12 h prior to incubation with probe-containing media. For imaging of MEFs, cells were grown to the desired confluency in the growth medium before direct incubation with probe-containing media.

For dual color imaging of Cu and Ca, HEK 293T cells were treated with 100 μM $CuCl_2$ or water in DMEM without phenol red for 12 h, incubated with 5 μM Calcium Green 1-AM (AAT Bioquest) in HBSS without $CaCl_2$ or $MgCl_2$ (Gibco) for 30 min at 37 °C, followed by incubation in HBSS without $CaCl_2$ or $MgCl_2$ for de-esterification for 30 min at 37 °C, and

incubation with 5 μM CPF1 or Ctrl-CPF1 in HBSS without $CaCl_2$ or $MgCl_2$ for 15 min at 37 °C prior to imaging in HBSS with 1 mM $CaCl_2$ without phenol red.

For colocalization experiments, cells were stained with 5 μM ER-Tracker Green (Thermo Fisher) in DMEM without phenol red for 15 min prior to incubation with 2 μM CCF1, CSF1, or CPF1 in DMEM without phenol red for 15 min at 37 °C. The medium was then replaced with fresh DMEM, and the cells were imaged with a 63× oil-immersion objective lens. ER-Tracker Green was excited at 488 nm, and emission was collected between 493 and 550 nm.

Supplementary Material

Refer to Web version on PubMed Central for supplementary material.

ACKNOWLEDGMENTS

We thank the National Institutes of Health (GM79465) for supporting this work. C.J.C. is an Investigator with the Howard Hughes Medical Institute. K.M.R.-T. and C.M.A. were partially supported by a Chemical Biology Training Grant from the National Institutes of Health (T32 GM066698). S.K. thanks TUBITAK for postdoctoral support. C.M.A. was supported by a Hertz Foundation Graduate Fellowship. We thank M. J. Petris (University of Missouri) for providing the MEF Atp7a knockout and wild-type cells.

REFERENCES

(1). Lippard SJ, and Berg JM (1994) Principles of Bioinorganic Chemistry, University Science Books, Mill Valley, CA.

(2). Tapiero H, Townsend DM, and Tew KD (2003) Trace elements in human physiology and pathology. Biomed. Pharmacother 57, 386–398. [PubMed: 14652164]

(3). Turski ML, Brady DC, Kim HJ, Kim BE, Nose Y, Counter CM, Winge DR, and Thiele DJ (2012) A novel role for copper in Ras/mitogen-activated protein kinase signaling. Mol. Cell. Biol 32, 1284–1295. [PubMed: 22290441]

(4). Brady DC, Crowe MS, Turski ML, Hobbs GA, Yao X, Chaikuad A, Knapp S, Xiao K, Campbell SL, Thiele DJ, and Counter CM (2014) Copper is required for oncogenic BRAF signalling and tumorigenesis. Nature 509, 492–496. [PubMed: 24717435]

(5). Krishnamoorthy L, Cotruvo JAJ, Chan J, Kaluarachchi H, Muchenditsi A, Pendyala VS, Jia S, Aron AT, Vander Wal MN, Guan T, Smaga LP, Farhi SS, New EJ, Lutsenko S, Chang CJ, and Ackerman CM (2016) Copper regulates cyclic AMP-dependent lipolysis. Nat. Chem. Biol 12, 586–592. [PubMed: 27272565]

(6). Halliwell B, and Gutteridge JM (1990) Role of free radicals and catalytic metal ions in human disease: an overview. Methods Enzymol 186, 1–85.

(7). Gaetke LM, and Chow CK (2003) Copper toxicity, oxidative stress, and antioxidant nutrients. Toxicology 189, 147–163. [PubMed: 12821289]

(8). Huffman DL, and O'Halloran TV (2001) Function, structure, and mechanism of intracellular copper trafficking proteins. Annu. Rev. Biochem 70, 677–701. [PubMed: 11395420]

(9). Luk E, Jensen LT, and Culotta VC (2003) The many highways for intracellular trafficking of metals. JBIC, J. Biol. Inorg. Chem 8, 803–809. [PubMed: 14517615]

(10). Robinson NJ, and Winge DR (2010) Copper metal-lochaperones. Annu. Rev. Biochem 79, 537–62. [PubMed: 20205585]

(11). Linz R, and Lutsenko S (2007) Copper-transporting ATPases ATP7A and ATP7B: cousins, not twins. J. Bioenerg. Biomembr 39, 403–407. [PubMed: 18000748]

(12). La Fontaine S, and Mercer JF (2007) Trafficking of the copper-ATPases, ATP7A and ATP7B: role in copper homeostasis. Arch. Biochem. Biophys 463, 149–167. [PubMed: 17531189]

(13). Kim BE, Nevitt T, and Thiele DJ (2008) Mechanisms for copper acquisition, distribution and regulation. Nat. Chem. Biol 4, 176–85. [PubMed: 18277979]

(14). Ayton S, Lei P, and Bush AI (2013) Metallostasis in Alzheimer's disease. Free Radical Biol. Med 62, 76–89. [PubMed: 23142767]

(15). Barnham KJ, Masters CL, and Bush AI (2004) Neurodegenerative diseases and oxidative stress. Nat. Rev. Drug Discovery 3, 205–14. [PubMed: 15031734]

(16). Savelieff MG, Lee S, Liu Y, and Lim MH (2013) Untangling amyloid-b, tau, and metals in Alzheimer's disease. ACS Chem. Biol 8, 856–865. [PubMed: 23506614]

(17). Matlack KE, Tardiff DF, Narayan P, Hamamichi S, Caldwell KA, Caldwell GA, and Lindquist S (2014) Clioquinol promotes the degradation of metal-dependent amyloid-b (Ab) oligomers to restore endocytosis and ameliorate Ab toxicity. Proc. Natl. Acad. Sci. U. S. A 111, 4013–4018. [PubMed: 24591589]

(18). Vonk WI, Kakkar V, Bartuzi P, Jaarsma D, Berger R, Hofker MH, Klomp LW, Wijmenga C, Kampinga HH, and van de Sluis B (2014) The Copper Metabolism MURR1 domain protein 1 (COMMD1) modulates the aggregation of misfolded protein species in a client-specific manner. PLoS One 9, e92408. [PubMed: 24691167]

(19). Xiao G, Fan Q, Wang X, and Zhou B (2013) Huntington disease arises from a combinatory toxicity of polyglutamine and copper binding. Proc. Natl. Acad. Sci. U. S. A 110, 14995–15000. [PubMed: 23980182]

(20). Valentine JS, Doucette PA, and Zittin Potter S (2005) Copper-zinc superoxide dismutase and amyotrophic lateral sclerosis. Annu. Rev. Biochem 74, 563–593. [PubMed: 15952898]

(21). Gaggelli E, Kozlowski H, Valensin D, and Valensin G (2006) Copper homeostasis and neurodegenerative disorders (Alzheimer's, prion, and Parkinson's diseases and amyotrophic lateral sclerosis). Chem. Rev 106, 1995–2044. [PubMed: 16771441]

(22). Seetharaman SV, Prudencio M, Karch C, Holloway SP, Borchelt DR, and Hart PJ (2009) Immature copper-zinc superoxide dismutase and familial amyotrophic lateral sclerosis. Exp. Biol. Med 234, 1140–1154.

(23). Sheng Y, Chattopadhyay M, Whitelegge J, and Selverstone Valentine J (2012) SOD1 aggregation and ALS: role of metallation states and disulfide status. Curr. Top. Med. Chem 12, 2560–2572. [PubMed: 23339308]

(24). Burkhead JL, and Lutsenko S (2013) The Role of Copper as a Modifier of Lipid Metabolism, in Lipid Metabolism (Baez RV, Ed.), pp 39–60, InTech, Rijeka, Croatia.

(25). Huster D, Purnat TD, Burkhead JL, Ralle M, Fiehn O, Stuckert F, Olson NE, Teupser D, and Lutsenko S (2007) High copper selectively alters lipid metabolism and cell cycle machinery in the mouse model of Wilson disease. J. Biol. Chem 282, 8343–8355. [PubMed: 17205981]

(26). Huster D, and Lutsenko S (2007) Wilson disease: not just a copper disorder. Analysis of a Wilson disease model demonstrates the link between copper and lipid metabolism. Mol. BioSyst 3, 816–824. [PubMed: 18000558]

(27). Vulpe C, Levinson B, Whitney S, Packman S, and Gitschier J (1993) Isolation of a candidate gene for Menkes disease and evidence that it encodes a copper-transporting ATPase. Nat. Genet 3, 7–13. [PubMed: 8490659]

(28). Kaler SG (2011) ATP7A-related copper transport diseases -emerging concepts and future trends. Nat. Rev. Neurol 7, 15–29. [PubMed: 21221114]

(29). Lutsenko S (2008) Atp7b$^{-/-}$ mice as a model for studies of Wilson's disease. Biochem. Soc. Trans 36, 1233–8. [PubMed: 19021531]

(30). Huster D, Hoppert M, Lutsenko S, Zinke J, Lehmann C, Mossner J, Berr F, and Caca K (2003) Defective cellular localization of mutant ATP7B in Wilson's disease patients and hepatoma cell lines. Gastroenterology 124, 335–345. [PubMed: 12557139]

(31). Huster D (2014) Structural and metabolic changes in Atp7b$^{-/-}$ mouse liver and potential for new interventions in Wilson's disease. Ann. N. Y. Acad. Sci 1315, 37–44. [PubMed: 24697742]

(32). Chang CJ (2015) Searching for harmony in transition-metal signaling. Nat. Chem. Biol 11, 744–747. [PubMed: 26379012]

(33). Chang CJ (2017) Bioinorganic Life and Neural Activity: Toward a Chemistry of Consciousness? Acc. Chem. Res 50, 535–538. [PubMed: 28945425]

(34). Dodani SC, Firl A, Chan J, Nam CI, Aron AT, Onak CS, Ramos-Torres KM, Paek J, Webster CM, Feller MB, and Chang CJ (2014) Copper is an endogenous modulator of neural circuit spontaneous activity. Proc. Natl. Acad. Sci. U. S. A 111, 16280–16285. [PubMed: 25378701]

(35). Dodani SC, Domaille DW, Nam CI, Miller EW, Finney LA, Vogt S, and Chang CJ (2011) Calcium-dependent copper redistributions in neuronal cells revealed by a fluorescent copper sensor and X-ray fluorescence microscopy. Proc. Natl. Acad. Sci. U. S. A 108, 5980–5. [PubMed: 21444780]

(36). Crabtree RH (1978) Copper (I): A possible olfactory binding site. J. Inorg. Nucl. Chem 40, 1453.

(37). Duan X, Block E, Li Z, Connelly T, Zhang J, Huang Z, Su X, Pan Y, Wu L, Chi Q, Thomas S, Zhang S, Ma M, Matsunami H, Chen G-Q, and Zhuang H (2012) Crucial role of copper in detection of metal-coordinating odorants. Proc. Natl. Acad. Sci. U. S. A 109, 3492–3497. [PubMed: 22328155]

(38). Palmer AE, and Tsien RY (2006) Measuring calcium signaling using genetically targetable fluorescent indicators. Nat. Protoc 1, 1057–1065. [PubMed: 17406387]

(39). Domaille DW, Que EL, and Chang CJ (2008) Synthetic fluorescent sensors for studying the cell biology of metals. Nat. Chem. Biol 4, 168–175. [PubMed: 18277978]

(40). Que EL, Domaille DW, and Chang CJ (2008) Metals in neurobiology: probing their chemistry and biology with molecular imaging. Chem. Rev 108, 1517–1549. [PubMed: 18426241]

(41). Nolan EM, and Lippard SJ (2009) Small-molecule fluorescent sensors for investigating zinc metalloneurochemistry. Acc. Chem. Res 42, 193–203. [PubMed: 18989940]

(42). Dean KM, Qin Y, and Palmer AE (2012) Visualizing metal ions in cells: an overview of analytical techniques, approaches, and probes. Biochim. Biophys. Acta, Mol. Cell Res 1823, 1406–1415.

(43). Carter KP, Young AM, and Palmer AE (2014) Fluorescent sensors for measuring metal ions in living systems. Chem. Rev 114, 4564–4601. [PubMed: 24588137]

(44). Aron AT, Ramos-Torres KM, Cotruvo JA, and Chang CJ (2015) Recognition- and Reactivity-Based Fluorescent Probes for Studying Transition Metal Signaling in Living Systems. Acc. Chem. Res 48, 2434–2442. [PubMed: 26215055]

(45). Shaner NC, Steinbach PA, and Tsien RY (2005) A guide to choosing fluorescent proteins. Nat. Methods 2, 905–9. [PubMed: 16299475]

(46). Giepmans BNG, Adams SR, Ellisman MH, and Tsien RY (2006) The fluorescent toolbox for assessing protein location and function. Science 312, 217–224. [PubMed: 16614209]

(47). Terai T, and Nagano T (2008) Fluorescent probes for bioimaging applications. Curr. Opin. Chem. Biol 12, 515–21. [PubMed: 18771748]

(48). Lavis LD, and Raines RT (2008) Bright ideas for chemical biology. ACS Chem. Biol 3, 142–155. [PubMed: 18355003]

(49). Fahrni CJ (2013) Synthetic fluorescent probes for monovalent copper. Curr. Opin. Chem. Biol 17, 656–662. [PubMed: 23769869]

(50). Cotruvo JA, Jr., Aron AT, Ramos-Torres KM, and Chang CJ (2015) Synthetic fluorescent probes for studying copper in biological systems. Chem. Soc. Rev 44, 4400–4414. [PubMed: 25692243]

(51). Ramos-Torres KM, Kolemen S, and Chang CJ (2016) Thioether Coordination Chemistry for Molecular Imaging of Copper in Biological Systems. Isr. J. Chem 56, 724–737.

(52). Liu J, and Lu Y (2007) A DNAzyme catalytic beacon sensor for paramagnetic Cu2+ ions in aqueous solution with high sensitivity and selectivity. J. Am. Chem. Soc 129, 9838–9839. [PubMed: 17645334]

(53). Wegner SV, Arslan H, Sunbul M, Yin J, and He C (2010) Dynamic copper (I) imaging in mammalian cells with a genetically encoded fluorescent copper(I) sensor. J. Am. Chem. Soc 132, 2567–2569. [PubMed: 20131768]

(54). Liu J, Karpus J, Wegner SV, Chen PR, and He C (2013) Genetically encoded copper(I) reporters with improved response for use in imaging. J. Am. Chem. Soc 135, 3144–3149. [PubMed: 23360467]

(55). Choi Y-A, Keem JO, Kim CY, Yoon HR, Heo WD, Chung BH, and Jung Y (2015) A novel copper-chelating strategy for fluorescent proteins to image dynamic copper fluctuations on live cell surfaces. Chem. Sci 6, 1301–1307. [PubMed: 29560216]

(56). Santo CE, Lam EW, Elowsky CG, Quaranta D, Domaille DW, Chang CJ, and Grass G (2011) Bacterial Killing by Dry Metallic Copper Surfaces. Appl. Environ. Microbiol 77, 794–802. [PubMed: 21148701]

(57). Ladomersky E, Khan A, Shanbhag V, Cavet JS, Chan J, Weisman GA, and Petris MJ (2017) Host and pathogen copper-transporting P-type ATPases function antagonistically during Salmonella infection. Infect. Immun 85, e00351–17. [PubMed: 28652309]

(58). Quaranta D, Krans T, Santo CE, Elowsky CG, Domaille DW, Chang CJ, and Grass G (2011) Mechanisms of Contact-Mediated Killing of Yeast Cells on Dry Metallic Copper Surfaces. Appl. Environ. Microbiol 77, 416–426. [PubMed: 21097600]

(59). Cusick KD, Minkin SC, Dodani SC, Chang CJ, Wilhelm SW, and Sayler GS (2012) Inhibition of Copper Uptake in Yeast Reveals the Copper Transporter Ctr1p As a Potential Molecular Target of Saxitoxin. Environ. Sci. Technol 46, 2959–2966. [PubMed: 22304436]

(60). Beaudoin J, Ioannoni R, López-Maury L, Bähler J, Ait- Mohand S, Guérin B, Dodani SC, Chang CJ, and Labbé S (2011) Mfc1 Is a Novel Forespore Membrane Copper Transporter in Meiotic and Sporulating Cells. J. Biol. Chem 286, 34356–34372. [PubMed: 21828039]

(61). Bernal M, Casero D, Singh V, Wilson GT, Grande A, Yang H, Dodani SC, Pellegrini M, Huijser P, Connolly EL, Merchant SS, and Krämer U (2012) Transcriptome Sequencing Identifies SPL7-Regulated Copper Acquisition Genes FRO4/FRO5 and the Copper Dependence of Iron Homeostasis in Arabidopsis. Plant Cell 24, 738–761. [PubMed: 22374396]

(62). Chun H, Sharma AK, Lee J, Chan J, Jia S, and Kim B-E (2017) The Intestinal Copper Exporter CUA-1 Is Required for Systemic Copper Homeostasis in Caenorhabditis elegans. J. Biol. Chem 292, 1–14. [PubMed: 27881675]

(63). Schrag M, Crofton A, Zabel M, Jiffry A, Kirsch D, Dickson A, Mao XW, Vinters HV, Domaille DW, Chang CJ, and Kirsch W (2011) Effect of cerebral amyloid angiopathy on brain iron, copper, and zinc in Alzheimer's disease. J. Alzheimers Dis 24, 137–149. [PubMed: 21187585]

(64). Öhrvik H, Nose Y, Wood LK, Kim B-E, Gleber S-C, Ralle M, and Thiele DJ (2013) Ctr2 regulates biogenesis of a cleaved form of mammalian Ctr1 metal transporter lacking the copper- and cisplatin-binding ecto-domain. Proc. Natl. Acad. Sci. U. S. A 110, E4279–E4288. [PubMed: 24167251]

(65). Huang CP, Fofana M, Chan J, Chang CJ, and Howell SB (2014) Copper transporter 2 regulates intracellular copper and sensitivity to cisplatin. Metallomics 6, 654–661. [PubMed: 24522273]

(66). Polishchuk EV, Concilli M, Iacobacci S, Chesi G, Pastore N, Piccolo P, Paladino S, Baldantoni D, van IJzendoorn SCD, Chan J, Chang CJ, Amoresano A, Pane F, Pucci P, Tarallo A, Parenti G, Brunetti-Pierri N, Settembre C, Ballabio A, and Polishchuk RS (2014) Wilson disease protein ATP7B utilizes lysosomal exocytosis to maintain copper homeostasis. Dev. Cell 29, 686–700. [PubMed: 24909901]

(67). Achard MES, Stafford SL, Bokil NJ, Chartres J, Bernhardt PV, Schembri MA, Sweet MJ, and McEwan AG (2012) Copper redistribution in murine macrophages in response to Salmonella infection. Biochem. J 444, 51–57. [PubMed: 22369063]

(68). Kashyap DR, Rompca A, Gaballa A, Helmann JD, Chan J, Chang CJ, Hozo I, Gupta D, and Dziarski R (2014) Peptidoglycan Recognition Proteins Kill Bacteria by Inducing Oxidative, Thiol, and Metal Stress. PLoS Pathog 10, e1004280. [PubMed: 25032698]

(69). Hong-Hermesdorf A, Miethke M, Gallaher SD, Kropat J, Dodani SC, Chan J, Barupala D, Domaille DW, Shirasaki DI, Loo JA, Weber PK, Pett-Ridge J, Stemmler TL, Chang CJ, and Merchant SS (2014) Subcellular metal imaging identifies dynamic sites of Cu accumulation in Chlamydomonas. Nat. Chem. Biol 10, 1034–1042. [PubMed: 25344811]

(70). Yang L, McRae R, Henary MM, Patel R, Lai B, Vogt S, and Fahrni CJ (2005) Imaging of the intracellular topography of copper with a fluorescent sensor and by synchrotron x-ray fluorescence microscopy. Proc. Natl. Acad. Sci. U. S. A 102, 11179–11184. [PubMed: 16061820]

(71). Morgan MT, Bagchi P, and Fahrni CJ (2011) Designed To Dissolve: Suppression of Colloidal Aggregation of Cu(I)-Selective Fluorescent Probes in Aqueous Buffer and In-Gel Detection of a Metallochaperone. J. Am. Chem. Soc 133, 15906–15909. [PubMed: 21916472]

(72). Morgan MT, McCallum AM, and Fahrni CJ (2016) Rational design of a water-soluble, lipid-compatible fluorescent probe for Cu(I) with sub-part-per-trillion sensitivity. Chem. Sci 7, 1468–1473. [PubMed: 28042469]

(73). Lim CS, Han JH, Kim CW, Kang MY, Kang DW, and Cho BR (2011) A copper(I)-ion selective two-photon fluorescent probe for in vivo imaging. Chem. Commun 7, 7146–7148.

(74). Zeng L, Miller EW, Pralle A, Isacoff EY, and Chang CJ (2006) A Selective Turn-On Fluorescent Sensor for Imaging Copper in Living Cells. J. Am. Chem. Soc 128, 10–11. [PubMed: 16390096]

(75). Dodani SC, Leary SC, Cobine PA, Winge DR, and Chang CJ (2011) A Targetable Fluorescent Sensor Reveals That Copper-Deficient SCO1 and SCO2 Patient Cells Prioritize Mitochondrial Copper Homeostasis. J. Am. Chem. Soc 133, 8606–8616. [PubMed: 21563821]

(76). Hirayama T, Van de Bittner GC, Gray LW, Lutsenko S, and Chang CJ (2012) Near-infrared fluorescent sensor for in vivo copper imaging in a murine Wilson disease model. Proc. Natl. Acad. Sci. U. S. A 109, 2228–2233. [PubMed: 22308360]

(77). Cao X, Lin W, and Wan W (2012) Development of a near-infrared fluorescent probe for imaging of endogenous Cu^{+} in live cells. Chem. Commun 48, 6247–6249.

(78). Arden-Jacob J, Frantzeskos J, Kemnitzer NU, Zilles A, and Drexhage KH (2001) New fluorescent markers for the red region. Spectrochim. Acta, Part A 57, 2271–83.

(79). Ohulchanskyy TY, Donnelly DJ, Detty MR, and Prasad PN (2004) Heteroatom Substitution Induced Changes in Excited-State Photophysics and Singlet Oxygen Generation in Chalcogenoxanthylium Dyes: Effect of Sulfur and Selenium Substitutions. J. Phys. Chem. B 108, 8668–8672.

(80). Calitree B, Donnelly DJ, Holt JJ, Gannon MK, Nygren CL, Sukumaran DK, Autschbach J, and Detty MR (2007) Tellurium Analogues of Rosamine and Rhodamine Dyes: Synthesis, Structure, 125Te NMR, and Heteroatom Contributions to Excitation Energies. Organometallics 26, 6248–6257.

(81). Kolmakov K, Belov VN, Bierwagen J, Ringemann C, Muller V, Eggeling C, and Hell SW (2010) Red-emitting rhodamine dyes for fluorescence microscopy and nanoscopy. Chem. -Eur. J 16, 158–166. [PubMed: 19950338]

(82). Egawa T, Koide Y, Hanaoka K, Komatsu T, Terai T, and Nagano T (2011) Development of a fluorescein analogue, TokyoMagenta, as a novel scaffold for fluorescence probes in red region. Chem. Commun 47, 4162–4.

(83). Koide Y, Urano Y, Hanaoka K, Terai T, and Nagano T (2011) Evolution of group 14 rhodamines as platforms for near-infrared fluorescence probes utilizing photoinduced electron transfer. ACS Chem. Biol 6, 600–8. [PubMed: 21375253]

(84). Kolmakov K, Wurm C, Sednev MV, Bossi ML, Belov VN, and Hell SW (2012) Masked red-emitting carbopyronine dyes with photosensitive 2-diazo-1-indanone caging group. Photochem. Photobiol. Sci 11, 522–32. [PubMed: 22218703]

(85). Kushida Y, Hanaoka K, Komatsu T, Terai T, Ueno T, Yoshida K, Uchiyama M, and Nagano T (2012) Red fluorescent scaffold for highly sensitive protease activity probes. Bioorg. Med. Chem. Lett 22, 3908–11. [PubMed: 22607681]

(86). Grimm JB, Sung AJ, Legant WR, Hulamm P, Matlosz SM, Betzig E, and Lavis LD (2013) Carbofluoresceins and Carborhodamines as Scaffolds for High-Contrast Fluorogenic Probes. ACS Chem. Biol 8, 1303–1310. [PubMed: 23557713]

(87). Lukinavicius G, Umezawa K, Olivier N, Honigmann A, Yang G, Plass T, Mueller V, Reymond L, Correa IR, Jr., Luo Z-G, Schultz C, Lemke EA, Heppenstall P, Eggeling C, Manley S, and Johnsson K (2013) A near-infrared fluorophore for live-cell super-resolution microscopy of cellular proteins. Nat. Chem 5, 132–139. [PubMed: 23344448]

(88). Fukazawa A, Suda S, Taki M, Yamaguchi E, Grzybowski M, Sato Y, Higashiyama T, and Yamaguchi S (2016) Phosphafluorescein: a red-emissive fluorescein analogue with high photo-bleaching resistance. Chem. Commun 52, 1120–1123.

(89). Zhou X, Lai R, Beck JR, Li H, and Stains CI (2016) Nebraska Red: a phosphinate-based near-infrared fluorophore scaffold for chemical biology applications. Chem. Commun 52, 12290–12293.

(90). Lavis LD (2017) Teaching Old Dyes New Tricks: Biological Probes Built from Fluoresceins and Rhodamines. Annu. Rev. Biochem 86, 825–843. [PubMed: 28399656]

(91). Weissleder R (2001) A clearer vision for in vivo imaging. Nat. Biotechnol 19, 316–7. [PubMed: 11283581]

(92). Magde D, Brannon JH, Cremers TL, and Olmsted J (1979) Absolute luminescence yield of cresyl violet. A standard for the red. J. Phys. Chem 83, 696–699.

(93). Wang Y, Zhu S, Weisman GA, Gitlin JD, and Petris MJ (2012) Conditional Knockout of the Menkes Disease Copper Transporter Demonstrates Its Critical Role in Embryogenesis. PLoS One 7, e43039. [PubMed: 22900086]

(94). Camakaris J, Danks DM, Ackland L, Cartwright E, Borger P, and Cotton RG (1980) Altered copper metabolism in cultured cells from human Menkes' syndrome and mottled mouse mutants. Biochem. Genet 18, 117–31. [PubMed: 7387619]

(95). La Fontaine SL, Firth SD, Camakaris J, Englezou A, Theophilos MB, Petris MJ, Howie M, Lockhart PJ, Greenough M, Brooks H, Reddel RR, and Mercer JF (1998) Correction of the copper transport defect of Menkes patient fibroblasts by expression of the Menkes and Wilson ATPases. J. Biol. Chem 273, 31375–31380. [PubMed: 9813047]

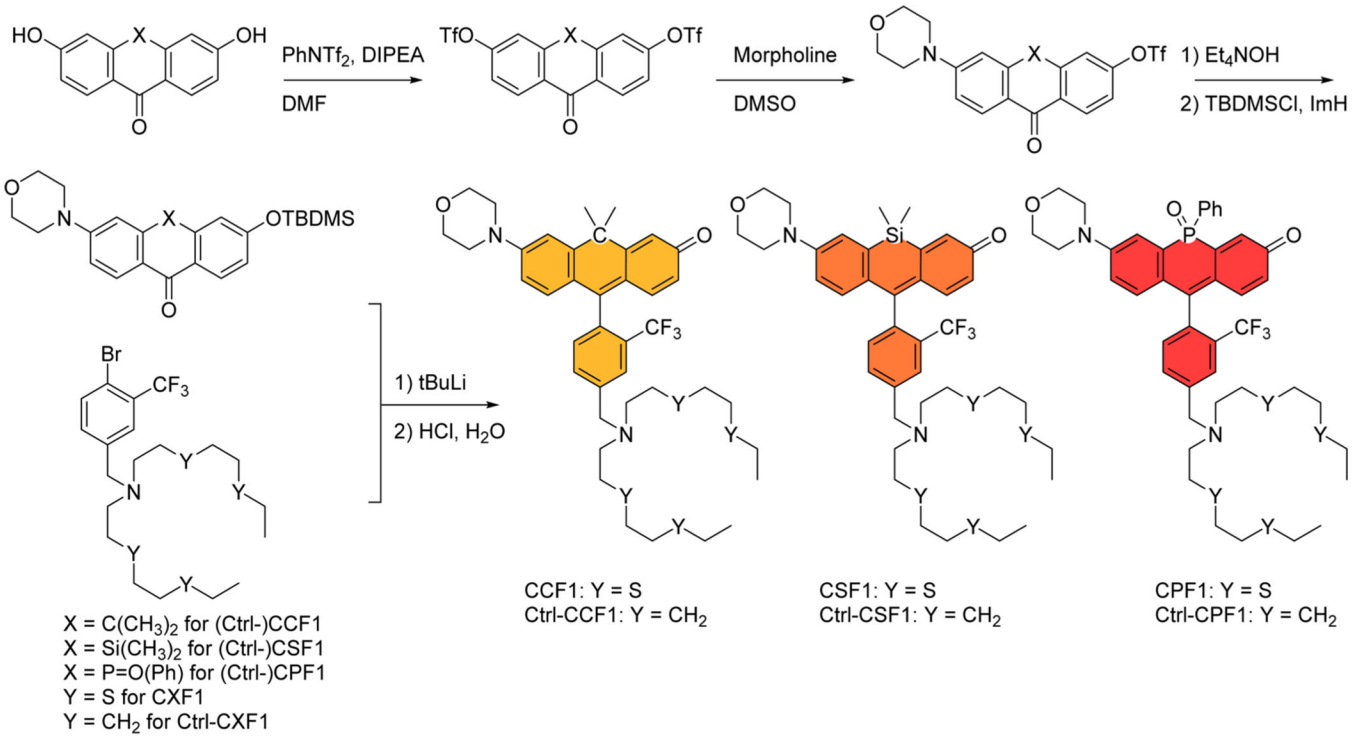

Scheme 1.

Synthesis and Structures of CCF1, CSF1, and CPF1 along with Their Control Analogs Ctrl-CCF1, Ctrl-CSF1, and Ctrl-CPF1

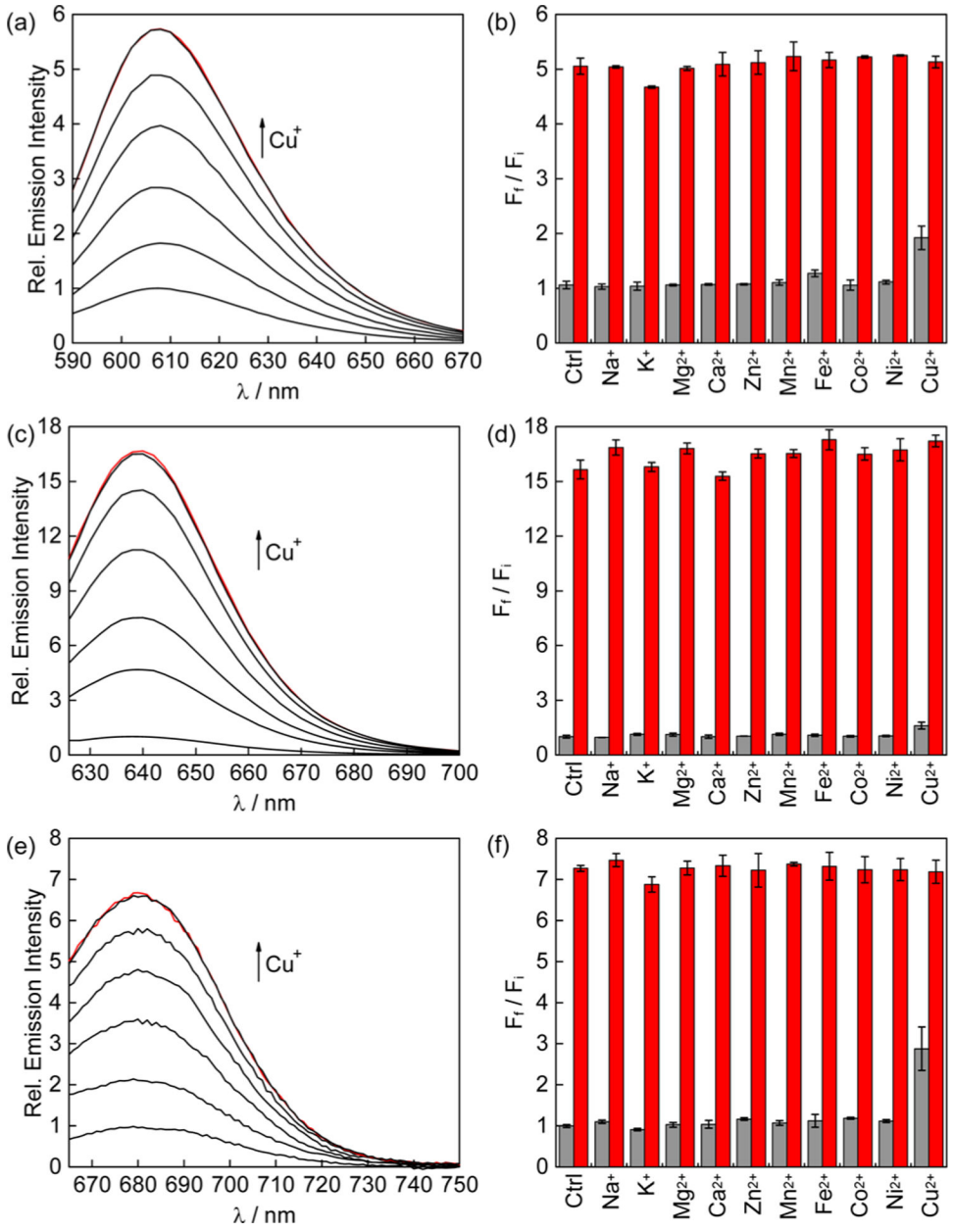

Figure 1.

Fluorescence turn-on responses of 1 μM (a) CCF1, (c) CSF1, and (e) CPF1 to Cu^+. Lines represent the addition of 0, 0.2, 0.4,0.6, 0.8, 1.0, and 1.2 μM $[Cu(MeCN)_4]PF_6$. Fluorescence responses of 1 μM (b) CCF1, (d) CSF1, and (f) CPF1 to various metal ions. Black bars represent the addition of an excess of the appropriate metal ion (2 mM for Na^+, K^+, Mg^{2+}, Ca^{2+}, and Zn^{2+} and 50 μM for other cations) to a 1 μM solution of probe. Red bars represent subsequent addition of 1 μM $[Cu(MeCN)_4]PF_6$. Bars represent the final integrated fluorescence response (F_f) over the initial integrated emission (F_i) shown as average ± s.d. (n = 3).

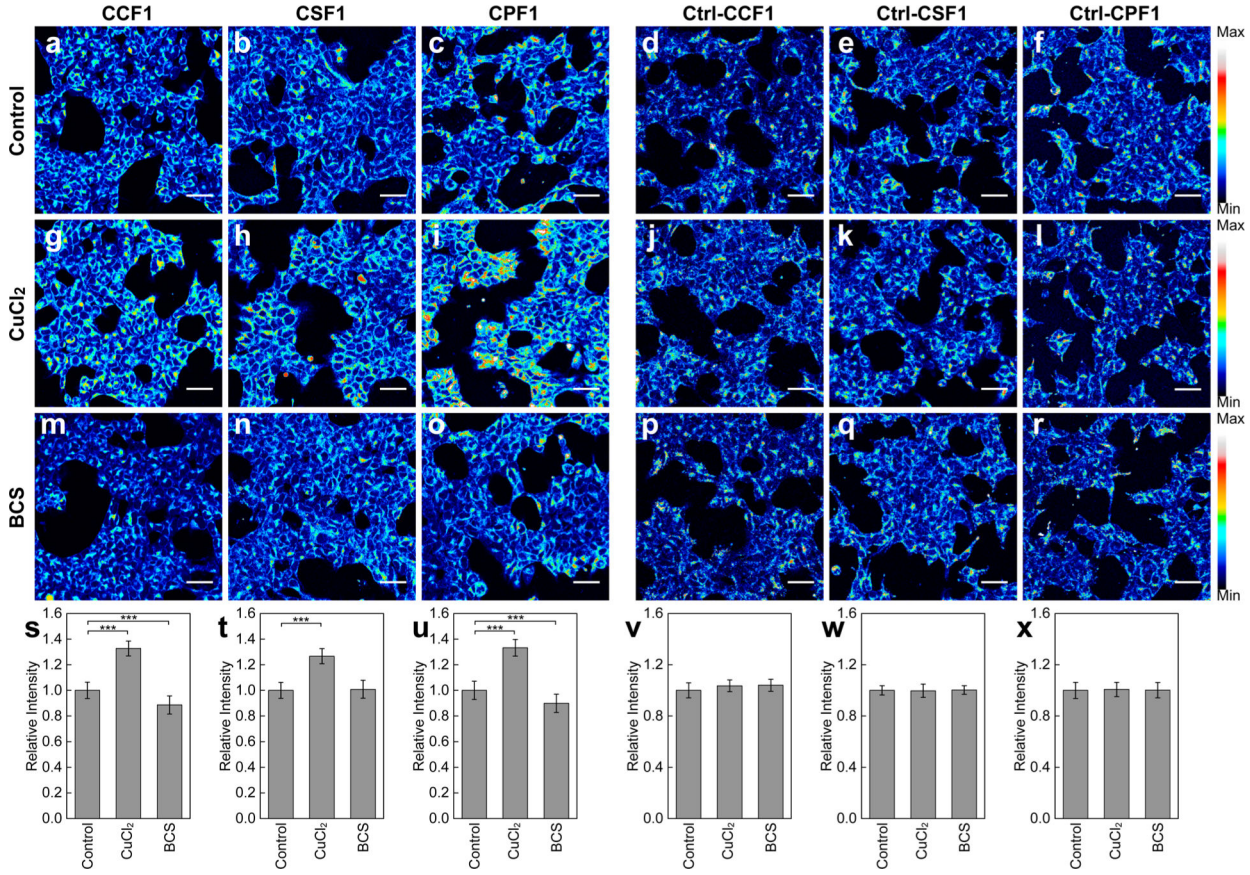

Figure 2.

Fluorescence imaging of labile copper pools in live HEK 293T cells with (a, g, m) CCF1, (b, h, n) CSF1, (c, i, o) CPF1, (d, j, p) Ctrl-CCF1, (e, k, q) Ctrl-CSF1, and (f, l, r) Ctrl-CPF1. Control cells (a–f) and cells incubated with (g–l) 100 μM $CuCl_2$ or (m–r) 500 μM BCS in the growth medium for 12 h at 37 °C were stained with 5 μM dye for 30 min at 37 °C in DMEM. Scale bars: 40 μm. (s–x) Quantification of fluorescence intensity of cells stained with CCF1, CSF1, CPF1, Ctrl-CCF1, Ctrl-CSF1, and Ctrl-CPF1, respectively. Data were normalized to control cells and shown as average ± s.d. (CXF, $n = 4$; Ctrl-CXF, $n = 3$). ***P ≤ 0.001; two-tailed Student's t test.

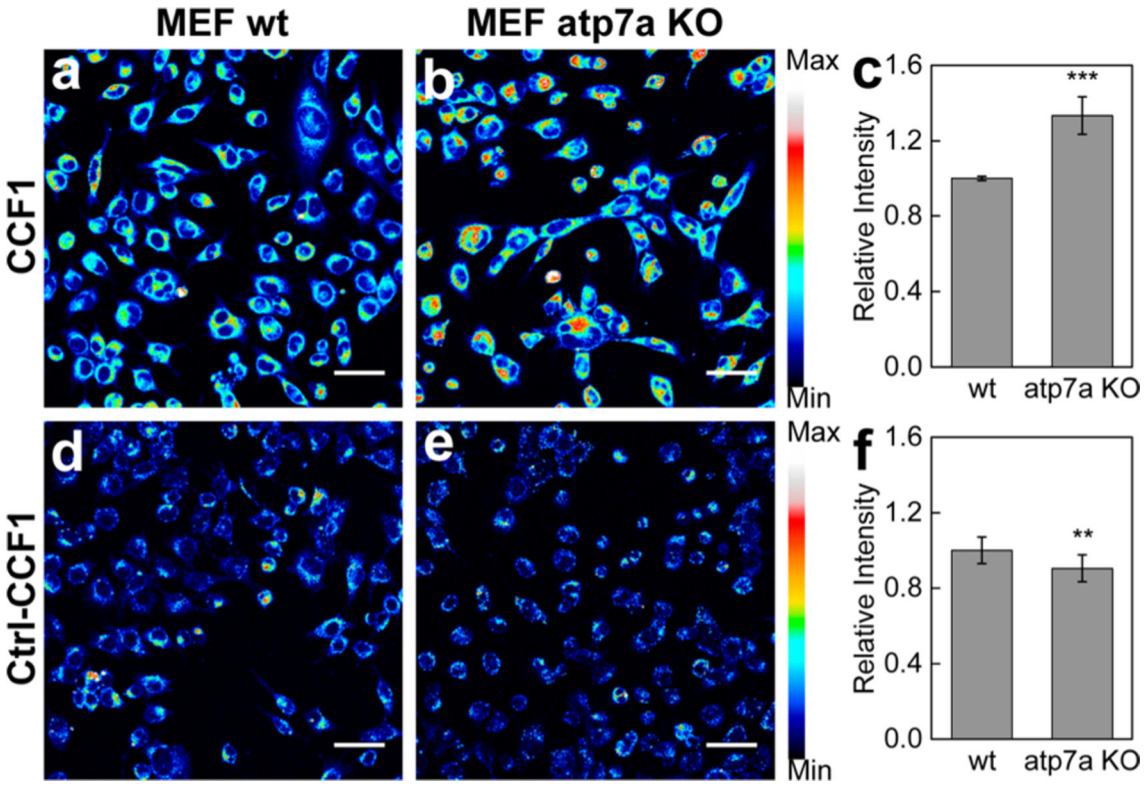

Figure 3.

Fluorescence imaging of labile copper pools in MEF wildtype (WT) and Atp 7a$^{-/-}$ knockout fibroblast cells with CCF1.(a) MEF WT cells and (b) MEF Atp7a$^{-/-}$ knockout cells were stained with 2 μM CCF1 for 10 min in DMEM, and their average fluorescence intensity was (c) quantified. (d) MEF WT cells and (e) MEF Atp7a$^{-/-}$ knockout cells were stained with 2 μM Ctrl-CCF1 for 10 min in DMEM and their average fluorescence intensity was (f) quantified. Scale bars: 40 μm. Data were normalized to MEF atp7a wt cells and shown as average ± s.d. (CCF1, n = 4; Ctrl-CCF1, n = 3). **P ≤ 0.01, ***P ≤ 0.001; two-tailed Student's t test.

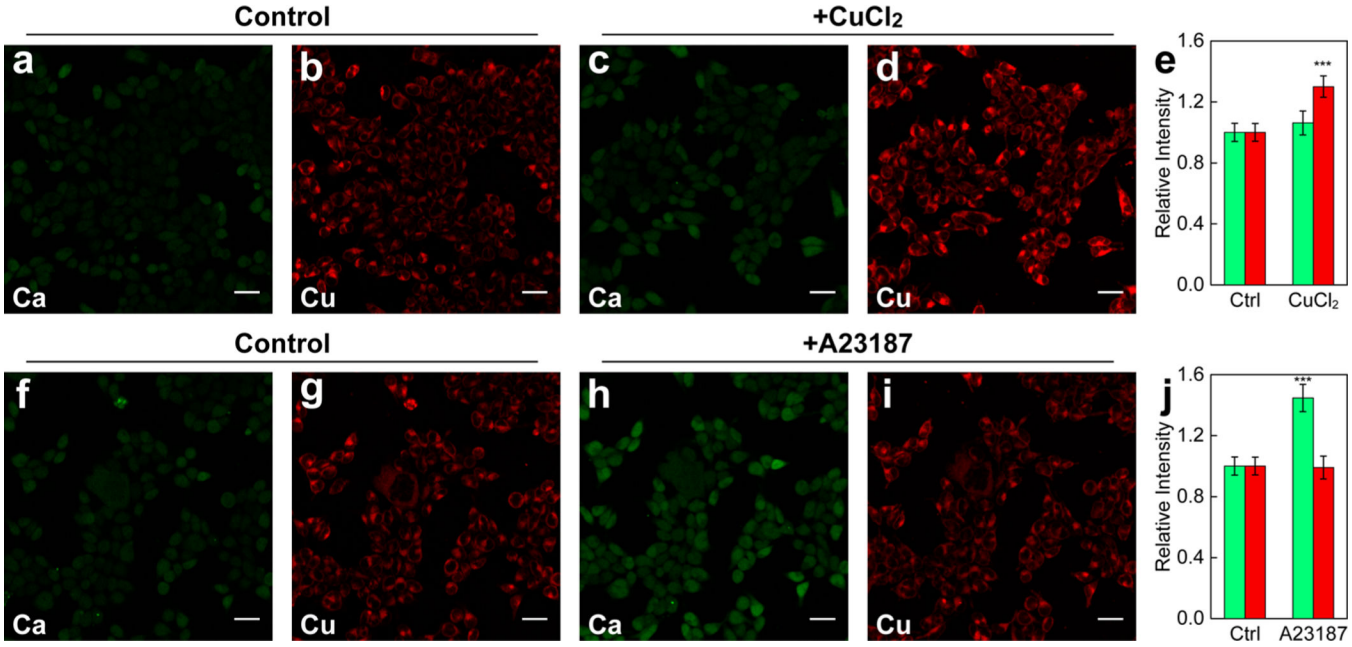

Figure 4.

Dual-channel fluorescence imaging of calcium and copper pools in live HEK 293T cells with Calcium Green-1 in the green channel (a, c, f,h) and CPF1 in the red channel (b, d, g, i). Control cells (a, b) and cells treated with 100 μM $CuCl_2$ for 12 h (c, d) were incubated with both dyes in HBSS and imaged; quantification is shown in e. Cells incubated with both dyes in HBSS prior to (f, g) and after (h, i) treatment of 1 μM calcium ionophore A23187 were imaged; quantification is shown in j. Green bars represent the Calcium Green-1 channel, and red bars are CPF1 channel. Scale bars: 40 μm. Data were normalized to control cells and shown as average ± s.d. (n = 4). ***P ≤ 0.001; two-tailed Student's t test.

Table 1.

Spectral Properties of CXF Copper Probes and Their Ctrl-CXF Control Analogs

	λ_{abs}/nm	λ_{em}/nm	$\varepsilon/10^4\ M^{-1}\ cm^{-1}$	Φ^a
CF3	510 and 550	557	3.3 and 3.7	0.026
CF3-Cu	534	557	6.9	0.219
Ctrl-CF3	510 and 545	557	4.7 and 4.7	0.007
CCF1	516	608	1.41	0.048
CCF1-Cu	580	608	2.05	0.30
Ctrl-CCF1	506	610	2.33	0.0083
CSF1	568	638	3.00	0.0041
CSF1-Cu	616	639	3.15	0.053
Ctrl-CSF1	531	638	1.99	0.0036
CPF1	569	679	1.76	0.00018
CPF1-Cu	654	680	1.93	0.0020
Ctrl-CPF1	568	674	1.72	0.00043

[a]Cresyl violet in methanol (Φ = 0.54)[92] was used as a standard.